Journal of the Optical Society of America A
OPTICS, IMAGE SCIENCE, AND VISION

Omnidirectional transformation-optics cloak made from lenses and glenses

Tomáš Tyc,[1] Stephen Oxburgh,[2] Euan N. Cowie,[2] Gregory J. Chaplain,[2] Gavin Macauley,[2] Chris D. White,[2] and Johannes Courtial[2,*]

[1]Institute of Theoretical Physics and Astrophysics, Masaryk University, Kotlarska 2, 61137 Brno, Czech Republic
[2]School of Physics & Astronomy, College of Science & Engineering, University of Glasgow, Glasgow G12 8QQ, UK
*Corresponding author: johannes.courtial@glasgow.ac.uk

Received 10 February 2016; revised 1 April 2016; accepted 1 April 2016; posted 4 April 2016 (Doc. ID 258587); published 9 May 2016

We present a design for an omnidirectional transformation-optics (TO) cloak comprising thin lenses and glenses (generalized thin lenses) [J. Opt. Soc. Am. A 33, 962 (2016)]. It should be possible to realize such devices in pixelated form. Our design is a piecewise nonaffine generalization of piecewise affine pixelated-TO devices [Proc. SPIE 9193, 91931E (2014); J. Opt 18, 044009 (2016)]. It is intended to be a step in the direction of TO devices made entirely from lenses, which should be readily realizable on large length scales and for a broad range of wavelengths.

OCIS codes: (080.2740) Geometric optical design; (080.3620) Lens system design; (230.3205) Invisibility cloaks; (240.3990) Micro-optical devices.
http://dx.doi.org/10.1364/JOSAA.33.001032

1. INTRODUCTION

Transformation optics (TO) [1,2] is the science of using a material structure to distort light-ray trajectories within the structure, thereby changing the apparent shape and/or size of any object inside it. The actual structure is said to be in physical space; the apparent structure as seen from the outside is called electromagnetic (EM) space. In the famous invisibility cloak [2], a physical-space void inside the structure and anything inside the void is made to appear infinitely small when viewed from outside the cloak (it is infinitely small in EM space), while any object behind the cloak is seen undistorted. This idea quickly took off, leading, for example, to different experimental realizations that use artificial metamaterial structures [3–7], natural crystals [8–10], and lenses and mirrors [11,12]. The ideas of TO have even been applied to other branches of physics, resulting, for example, in transformation thermodynamics [13,14], acoustic cloaking [15], elastic cloaking [16], and seismic cloaking [17].

The original suggestion was to realize TO devices using metamaterials, engineered structures with subwavelength-size features that allow their optical properties to be controlled, but it was quickly realized that such structures that work for all visible light and on macroscopic length scales would be difficult to realize. The reasons include the immense practical difficulties of manufacturing macroscopic, three-dimensional, spatially varying, bespoke nanostructures. There are also fundamental difficulties: ideal cloak structures have been built, but only on the scale of a few wavelengths (e.g., [7]), and the requirements on loss and bandwidth limitations that would allow significant size increases are daunting [18–20].

These difficulties led researchers to investigate alternative realizations [8–12] that are much easier to fabricate and that work for all visible light and at macroscopic length scales, but at the cost of compromising performance. Approximations of the material properties have been shown to introduce visible imperfections [21–26]; a number of the simplified devices work only for light incident from a limited range of directions, and in all cases the cloaking is "ray-optical," which means that these cloaks alter the phase of transmitted light.

Our own interest in TO stems from our research into light-ray-direction-changing microstructured sheets, called telescope windows, that can be combined into approximations to TO devices. A telescope window [27] comprises pairs of confocal microlens arrays [28,29] in which pairs of microlenses—one from each array—form telescopes that act as the "pixels" of the sheet. It can be shown that the light-ray-direction changes that can be achieved in this way—pixelated generalized refraction—could lead to wave-optically forbidden light-ray fields if the sheets were not pixelated [27,30]. The generalized laws of refraction that can be achieved in this way, albeit only in pixelated form, allow very general stigmatic imaging.

We recently defined a *glens* to be a planar interface that changes light-ray direction like an idealized thin lens, but generalized to have two independent focal lengths on the two sides of the lens [31]. If a glens is realized, approximately, in the form of a telescope window, then due to the pixelation the imaging is not stigmatic, but integral [32], and the approximate glens has other imperfections, such as the appearance of additional, and usually unwanted, images [33,34]. These imperfections are the subject of our current optical engineering efforts. On the plus side, telescope windows can be manufactured inexpensively on meter scales [35], and they work for all visible light.

We recently investigated the imaging properties of glenses in the homogeneous limit [36] and showed that these are so general that structures of homogeneous glenses can form omnidirectional TO devices [37,38]. Realizations of such devices in terms of telescope windows do not preserve the phase of transmitted light and are, therefore, merely ray-optical. As such, they have all the advantages and disadvantages of the telescope windows themselves, including integral imaging instead of stigmatic imaging, a limited field of view, and additional images. They will benefit significantly from improved optical engineering of the individual telescope windows. What sets them apart from other ray-optical TO devices is that they can be built cheaply, on large length scales. Here, we present an example of an omnidirectional TO cloak composed of inhomogeneous glenses and thin lenses.

The structure of this paper is as follows. First, in Section 2, we review the properties of glenses. In Section 3 we introduce a physical-space structure formed by glenses, and the corresponding EM-space structure. It contains a central region whose size differs in physical and EM space; in the theoretical limit when the size of the EM-space region is zero, the structure is a ray-optical cloak.

We then show that the structure indeed maps between physical and EM space as intended. Specifically, we show that any possible combination of surfaces that a ray traversing the cloak can encounter images every point back to itself. Assuming that the structure images as intended, we construct, in Section 4, the cardinal points of these glenses and show that a few of the glenses are actually lenses. Using the cardinal points we then show, in Section 5, that the structure indeed images as intended, and that our earlier assumption is therefore true and our argument consistent. In Section 6, we confirm these results using ray-tracing simulations of the cloak. Section 7 is a concluding discussion of our findings.

2. REVIEW OF GLENSES

Glenses have recently been defined to be planar interfaces that change the direction of transmitted light rays like ideal thin lenses that possess different focal lengths on the two sides of the interface [31]. Like thin lenses, glenses do not offset the position of transmitted light rays. The generalization from a thin lens to a glens at first appears rather small, but it is this small generalization that makes the resulting interfaces the most general imaging elements of their kind: it can be shown that glenses are the most general planar light-ray-direction-changing interfaces that image all of object space into all of image space and vice versa (it is a bijection) [39]. In fact, as curved light-ray-direction-changing interfaces can bijectively map object space into image space only trivially [40], glenses are *the* most general nontrivial light-ray-direction-changing interfaces (of any shape) that image between all of object space and image space.

Like a thin lens, a glens has an optical axis that is perpendicular to the plane of the glens and on which all the principal points lie. Unlike a thin lens, the two sides of a glens are different, which is why it is important to identify the sides. In Ref. [31] this is done by placing on the optical axis an axis of a Cartesian coordinate system, with its origin in the glens plane, and labeling the two sides of the glens by the sign of this coordinate there. The corresponding axial coordinate is called a. Light rays traveling on the side of the glens where a is positive are said to be traveling in positive space; those on the other side are said to be traveling in negative space.

Figure 1 shows a diagrammatic representation of a glens, its optical axis, its cardinal points, and different principal rays. Following one of the conventions introduced in Ref. [31], the positive side of the glens is identified by a "+" on that side of the line indicating the glens plane, and the negative side is identified by a "−." Three types of principal ray are shown: type 1 is parallel to the optical axis in negative space, and passes through the positive focal point, F^+, in positive space; type 2 passes through the negative focal point, F^-, in negative space, and is parallel to the optical axis in positive space; and type 3, which travels in the direction of the glens's nodal point, N, and passes straight through the glens. The two focal points and the nodal point, together with the principal point, P, which lies at the intersection between the glens plane and the optical axis, are the cardinal points of the glens.

A glens is fully characterized by its a axis and the positive and negative focal lengths, f^+ and f^-, which are defined as the a coordinates of the corresponding focal points. Using this convention, a thin lens with focal length f is a glens with $f^- = -f$ and $f^+ = f$. The a coordinate of the nodal point, N, is defined as the *nodal distance*, n, which is related to the focal lengths by the equation [31]

$$n = f^- + f^+. \tag{1}$$

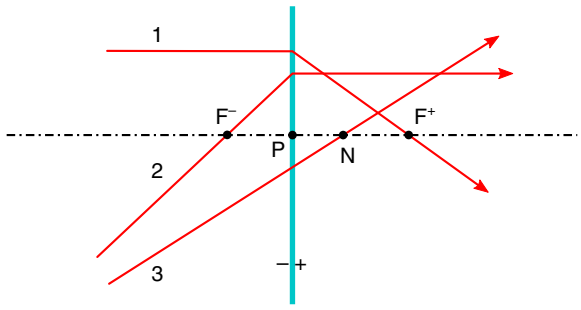

Fig. 1. Cardinal points and principal rays of a glens. The glens is indicated by the thick cyan vertical line through point P. The dashed–dotted horizontal line is the optical axis. The positive and negative sides of the glens are indicated with a "+" and a "−" on the corresponding side of the glens. N is the nodal point, P is the principal point, and F^- and F^+ are the focal points in negative and positive space, respectively. The rays (red arrows), which pass through the positive (ray 1) and negative (ray 2) focal points and through the nodal point (ray 3), are all examples of principal rays.

The light-ray-direction change in glenses is of a type that can lead to wave-optically forbidden light-ray fields [30], in which case it is not physically realizable. But if the light-ray-direction change is accompanied by a suitable ray offset, it can become realizable in those cases. If the ray offset is sufficiently small, it can be invisible. A Gabor superlens [41,42], an example of a telescope window, can be seen as an approximation to a glens that introduces such a small ray offset. The individual telescopes change light-ray direction as required, but also offset the rays on the scale of the aperture size of the individual telescopes. The telescopes can be seen as the pixels of the Gabor superlens, which is why we refer to it as a pixelated realization of a glens.

3. CLOAK STRUCTURE

Figure 2 sketches a two-dimensional structure of glenses. (We will generalize this structure to three dimensions in due course.) It consists of four outer glenses, located on the sides of an outer square of side length L, four inner glenses, located on the sides of an inner square of side length aL that shares its center and orientation with the outer square, and four diagonal glenses linking corresponding corners of the outer and inner squares.

The glenses divide physical space into polygonal regions, called R_0 (the outside of the device), R_1 to R_4, and R_5 (the inside of the inner square). Each glens separates two of these regions; the glens separating regions R_i and R_j is labeled G_{ij}. The vertices of the polygonal regions, where three or more regions (R_i, R_j, R_k, …) meet, are labeled $V_{ijk\ldots}$.

Figure 2 also sketches the structure of the corresponding EM space. The EM-space equivalent of the outer square coincides with its physical-space counterpart; the EM-space equivalent of the inner square is a smaller square of side length $a'L$ whose center and orientation coincide with those of the other squares. The vertices of the EM-space polygons are labeled such that vertex $V'_{ijk\ldots}$ is the point where the EM-space counterparts of regions R_i, R_j, R_k, …, meet.

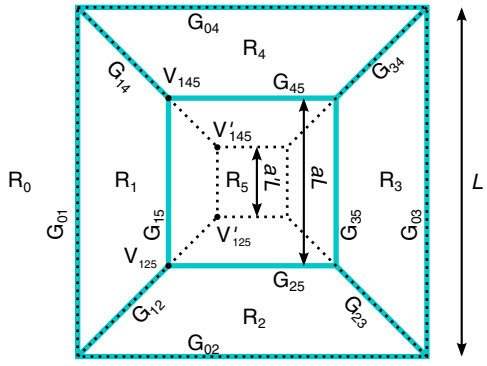

Fig. 2. Structure of a two-dimensional square cloak in physical space (solid cyan lines) and EM space (dotted black lines). Physical space is divided into six polygon-shaped regions, R_0 to R_5. Region R_0 is the outside of the cloak, in which physical space and EM space are identical; region R_5 is the inside of the cloak. Each straight line dividing two regions represents a glens; the glens separating regions R_i and R_j is called G_{ij}. A few of the vertices of the regions are also marked. Three or more regions meet there; the vertex where regions R_i, R_j, R_k, … meet is labeled $V_{ijk\ldots}$.

The two-dimensional structure can be generalized to three dimensions by replacing the glenses on the sides of concentric inner and outer squares with glenses on the faces of concentric inner and outer cubes, and by replacing the diagonal glenses that link corresponding corners of the inner and outer squares with glenses that link corresponding edges of the inner and outer cubes. There are 12 glenses that cover cube faces, and 12 that link corresponding edges. This glens structure now divides physical space into eight polygonal regions, namely, the outside, the inside of the inner cube, and six regions, each of which is sandwiched between corresponding faces of the inner and outer cubes. The EM-space equivalent of the outer cube coincides with its physical-space counterpart, and the EM-space counterpart of the inner cube has side length $a'L$ and shares its orientation and center with the other cubes.

4. CONSTRUCTION OF THE CARDINAL POINTS

We now construct the cardinal points of all glenses in the cloak structure described in the previous section.

First we analyze the outer glenses. For simplicity, we choose them all to be the same, giving the cloak cubic symmetry. It is therefore enough to analyze one of these glenses, namely, the left glens, G_{01}. It images the point V_{145} to V'_{145}, and V_{125} to V'_{125}. Its nodal point must therefore lie at the intersection of the straight lines $V_{145}V'_{145}$ and $V_{125}V'_{125}$, which is the center of the cloak, marked N in Fig. 3(a). By symmetry, N is therefore the nodal point of all outer glenses, and as a glens's nodal point always lies on the glens's optical axis, the optical axes of all outer glenses pass through N.

We can calculate the other cardinal points as follows. Figure 3(a) shows two rays, marked 1 and 2, which are incident from the left in the direction of point V'_{145}. The left glens, G_{01}, redirects them such that they travel in the direction of V_{145}. Ray 1 is chosen such that it is initially parallel to the optical axis (which is perpendicular to the glens plane and passes through N), which means it (or its straight-line continuation) passes through the positive focal point, F^+_{01}, after redirection. F^+_{01} also lies on the optical axis, which fully determines its position. Ray 2 is chosen such that it is parallel to the optical axis after redirection, which means that, before redirection, it (or its straight-line continuation) must have passed through the negative focal point, F^-_{01}. Like F^+_{01}, F^-_{01} lies on the optical axis, which again fully determines its position.

Next, we analyze the left inner glens, G_{15}, which is representative of all inner glenses. We consider a light ray incident on the left outer glens along a straight line through N. Light ray 3 in Fig. 3(b) is such a ray. Because N is the nodal point of the left outer glens, the ray passes straight through, intersecting the left inner glens at I_1. On the other side, after transmission through the right outer glens G_{03}, it must continue along the same straight-line trajectory. But this passes through the nodal point of that glens also, so the ray must have passed straight through it, which means it must have intersected the right inner glens G_{35} at I_2. Between the inner glenses, the ray must have traveled from I_1 to I_2, which means that it must have traveled along its original straight-line trajectory there. Thus, the inner glenses have not deflected that ray, so it must pass through the nodal point of both inner glenses.

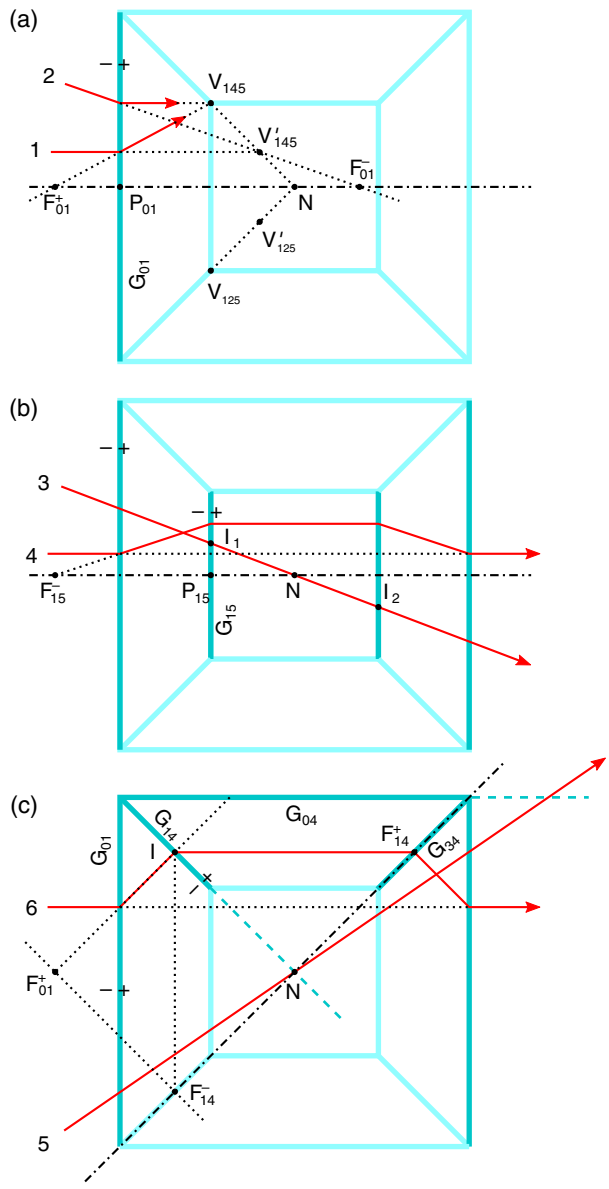

Fig. 3. Construction of the cardinal points of the glenses that form the cloak shown in Fig. 2. (a) Outer glenses, (b) inner glenses, and (c) diagonal glenses.

Repeating this argument for other rays through N leads to the result that N is the nodal point of all inner glenses also. This means that the optical axes of all inner glenses pass through N.

Ray 4 in Fig. 3(b) allows construction of the object-sided focal point F_{15}^{+} of glens G_{15}. The ray is constructed such that it travels initially parallel to the optical axis shared by the left and right inner and outer glenses before passing first through the left outer and inner glenses, then through the right inner and outer glenses. By symmetry, between the inner glenses it also travels parallel to the optical axis. When the ray hits the left outer glens, G_{01}, arriving from the negative side and traveling parallel to the optical axis, it gets redirected such that it subsequently passes through the positive focal point F_{01}^{+}. It then hits the left inner glens, G_{15}, from the negative side, which redirects it such that it is afterward parallel to the optical axis. This means that it must have come from the direction of the negative focal point, F_{15}^{-}. Considering rays of this type that initially travel at different distances from the optical axis leads to the result that the position of the negative focal point F_{15}^{-} of G_{15} coincides with that of the positive focal point F_{01}^{+} of G_{01}. The location of the positive focal point F_{15}^{+} can be constructed using the locations of F_{15}^{-}, N, and the relationship between the focal distances and the nodal distance [Eq. (1)]. The cardinal points of the glenses on the other inner glenses can be found by symmetry.

Before we proceed further, we notice a useful property of a system of glenses that will be used extensively below. In particular, to find the imaging properties of a particular glens, we may use rays that do not actually pass through that glens but that would do so if the glens were extended beyond its actual size. This follows from the fact that the image of a given point created by the glens is determined uniquely by any portion of that glens, and does not change if the glens is extended.

We can now apply this principle to analyze glens G_{14}, which is representative of the diagonal glenses. To do that, we extend glenses G_{14} and G_{04}; the relevant extensions are shown as dashed lines in Fig. 3(c). This way, ray 5 now intersects all three glenses G_{01}, G_{14}, and G_{04}. As this ray passes through N, which is the nodal point of glenses G_{01} and G_{04}, it passes through them undeviated. However, for the ray to continue along its original straight-line trajectory after transmission through all three glenses, it has to be undeviated by G_{14} also, so the nodal point of G_{14} must lie somewhere along the ray. The same argument applies if we rotate ray 5 slightly around N, which implies that N is the nodal point of G_{14}. This way we see that N is the nodal point of *all* glenses of the cloak. Further, N lies on (the continuation of) G_{14}, and so G_{14} and the other diagonal glenses G_{12}, G_{23}, and G_{34} are actually lenses.

We also employ ray 6 that is normally incident on G_{14} at position I from the direction of F_{01}^{+}. That means that it must have been normally incident on G_{01}. After transmission through the cloak, it must continue along its original straight-line trajectory. For symmetry reasons, between G_{14} and G_{34} the ray must therefore have the same direction with which it was incident on G_{01} [horizontal in Fig. 3(c)]. However, as the ray was normally incident on G_{14}, it must pass through image-sided focal point F_{14}^{+} after transmission through it. Point F_{14}^{+} can therefore be constructed as the intersection between this ray and the optical axis of lens G_{14}, shown as the dashed–dotted line in Fig. 3(c). As G_{14} is a lens, the other focal point, F_{14}^{-}, is located the same distance from N, but on the opposite side, on the optical axis.

We note that the negative focal plane of G_{14}, shown in Fig. 3(c) as a dotted line through F_{14}^{-} and parallel to G_{14}, passes through point F_{01}^{+} (and therefore also F_{15}^{-}). This is the case because G_{14} is a lens, and so F_{14}^{-} is located on the optical axis of G_{14} and the same distance from it as F_{14}^{+}, but on the opposite side.

5. PROOF OF IMAGING OF ALL POINTS BACK TO THEMSELVES

Having found the parameters of all the glenses of the cloak, we also have to show that any spatial point will be imaged to itself

by the cloak, no matter which possible combination of surfaces it may encounter upon traversing the cloak. We do this in two steps. First, we show that any combination of glenses that a ray may encounter images every point. Second, we show that the image of every point coincides with the point itself.

The first step is easy: a glens images any point in object space into a corresponding point in image space [39]. Transmission through any other glenses simply re-images the image from the previous glens(es). As all surfaces in the cloak are glenses, any combination of these automatically images any point.

The second step is more complicated. We use the result from the first step, namely, that any point is being imaged. This implies that all light rays that intersect at a point Q (the object) before transmission through the cloak again intersect at a point Q' (the image) after transmission. To find where this image position is, we need only to find the intersection of any two of these rays; all others then automatically intersect there, also. We pick each of the rays such that it is a member of a family of light rays that is sufficiently general so that the object position becomes completely arbitrary, and we do this separately for any combination of glenses that may be encountered.

Figure 4(a) investigates transmission through the left and right inner and outer glenses, i.e., for the glens combination (G_{01}, G_{15}, G_{35}, G_{03}). We choose the first ray, marked 1 in Fig. 4(a), to pass through N, which is the nodal point of all glenses in the cloak and which, therefore, passes through the cloak undeviated. The four glenses under consideration have a common optical axis, and it is advantageous to choose the second ray [ray 2 in Fig. 4(a)] as being initially parallel to this optical axis. This ray is redirected by G_{01} such that it passes through F_{01}^{+}, whose position is identical to that of F_{15}^{-} (see Section 4), and so it becomes parallel again to the optical axis of G_{15} after passing through G_{15}. The same happens in reverse when the ray continues through glenses G_{35} and G_{03}. This way, beyond the cloak, both rays 1 and 2 continue along their original straight-line trajectories, which means that image Q' of their intersection point Q coincides with Q itself. Moreover, ray 1 can be rotated around N while ray 2 can be shifted sideways, to move their intersection Q arbitrarily. We thus see that the combination of these four glenses images as required.

Figure 4(b) deals with the glens combination (G_{01}, G_{14}, G_{34}, G_{03}). As before, we pick a ray, namely, ray 3, that passes through the common nodal point N, so it is undeviated. We choose ray 4 to be initially parallel to the optical axis of glens G_{01}, but, unlike ray 6 in Fig. 3(c), its height can be chosen arbitrarily. As ray 4 is incident parallel to the optical axis of glens G_{01} from the negative side, it will be redirected onto a straight

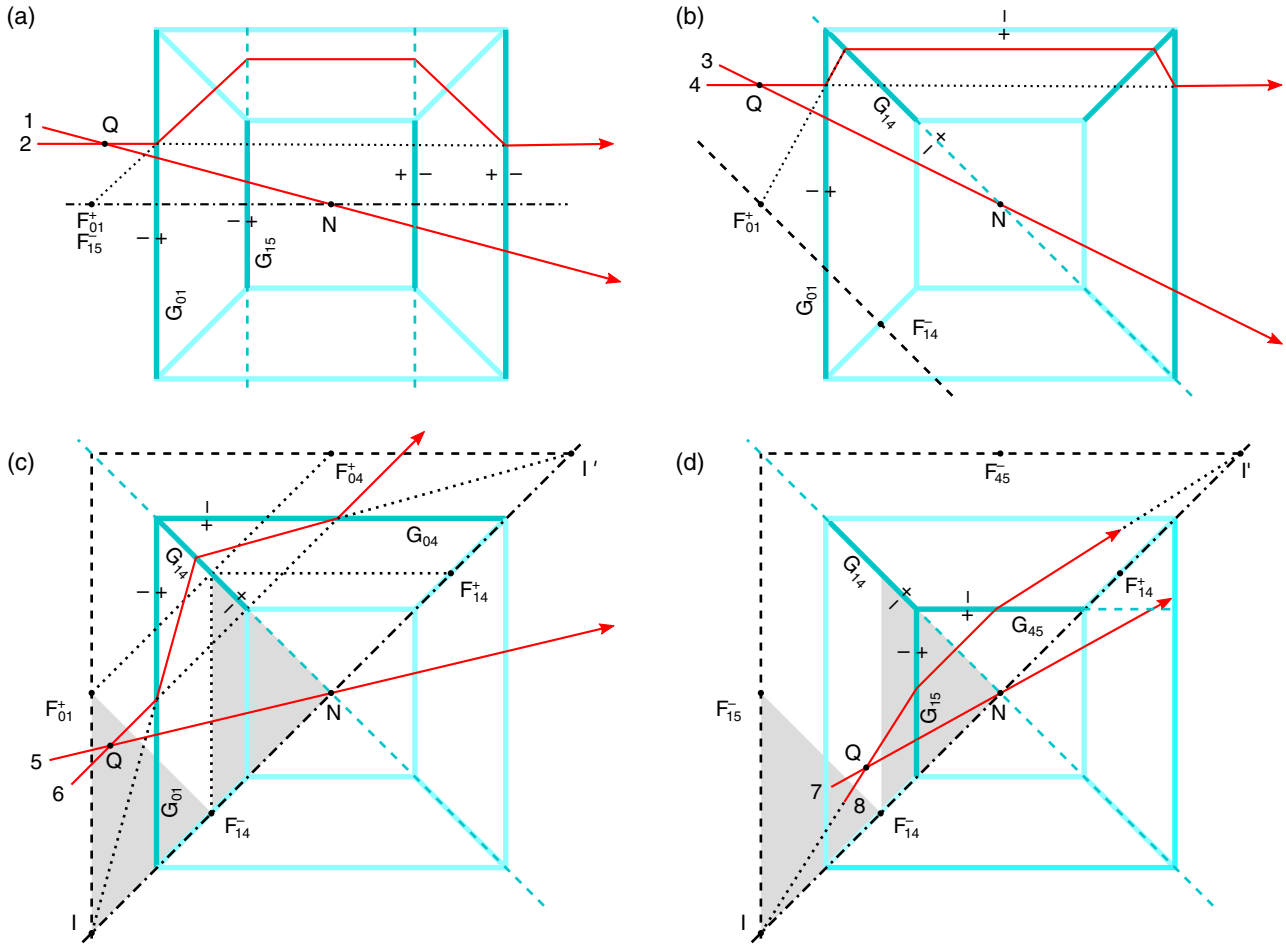

Fig. 4. Imaging properties of the glens combinations encountered along different types of ray trajectories through the cloak.

line through F_{01}^{+}. However, at the end of the previous section we observed that F_{01}^{+} lies in the negative-sided focal plane of lens G_{14}, which means that G_{14} redirects ray 4 such that it is parallel to the straight line connecting F_{01}^{+} and N, which in Fig. 4(b) is a horizontal line. It gets redirected symmetrically by the two glenses on the right, which means that it will eventually travel along its initial straight-line trajectory. The rest of the argument goes the same way as in the previous case.

Figure 4(c) treats the glens combination (G_{01}, G_{14}, G_{04}). Ray 5 passes through N again and is hence undeviated. We choose ray 6 to be initially parallel with the optical axis of G_{14}, shown as a dashed–dotted diagonal line. To find its direction beyond G_{01}, we use the fact that two initially parallel rays incident upon a glens continue beyond it such that their prolongations pass through a common point, I, in the image-sided focal plane. This image-sided focal plane is parallel to G_{01} and contains focal point F_{01}^{+}, and is shown as a vertical dashed line in Fig. 4(c). Point I can be found as the intersection of this image-sided focal plane with the straight line with the initial direction of ray 6 and passing through N, namely, the optical axis of G_{14}. To find out where on the optical axis of G_{14} point I lies, we consider the triangle with vertices I and F_{01}^{+} and angles 45° at these vertices [the lower shaded triangle in Fig. 4(c)]. Its third vertex with angle 90° then coincides with the focal point F_{14}^{-} of glens G_{14}, which follows from the fact that F_{01}^{+} lies in the negative focal plane of G_{14}. Next we note that this triangle is congruent with the triangle with the same angles and with vertices F_{14}^{-} and N (the second shaded triangle in the figure; in 3D, both triangles lie in the plane containing the optical axes of G_{01}, G_{14}, and G_{04}), so the distance of point I from nodal point N of lens G_{14} is twice the focal length of G_{14}. Consequently, point I will be imaged by lens G_{14} to a point I' on its optical axis a distance of two focal lengths behind N ($4f$ imaging). This ensures that the ray trajectory is mirror symmetric with respect to the plane of G_{14}, and as the ray was incident along a normal to G_{14}, it leaves along the same normal.

Finally, we use a very similar argument to demonstrate the equivalence of transmission through lens G_{14} and through the combination of glenses G_{15} and G_{45}. We will investigate two particular types of ray that can be made to intersect anywhere and show that diagonal lens G_{14} changes both rays in the same way as the combination of G_{15} and G_{45}. It will then follow that they image any point to the same position, which will, in turn, show that they redirect any ray in the same way. Figure 4(d) shows the geometry. As usual, we pick a ray, here ray 7, to pass through the common nodal point N, so it passes through undeviated. As the other ray, here ray 8, we pick a ray that approaches from point I defined above that is located two focal lengths in front of lens G_{14}. Lens G_{14} will simply redirect it such that it passes through point I', as has been shown above. As for glens G_{15}, the ray approaches it from the direction of point I in its negative focal plane, and it therefore is redirected into the same direction as any other ray that approaches G_{15} from I. Taking this other ray as the one passing through N, we see that G_{15} will redirect ray 2 to become parallel to the optical axis of G_{14}, shown as the dashed–dotted diagonal. By symmetry, the ray is then redirected by glens G_{45} toward I'. This completes the proof of equivalence of lens G_{14} and the pair of glenses G_{15} and G_{45}.

We see that any spatial point is imaged to itself by any possible combination of glenses that a ray can penetrate when passing through the cloak. This shows that the device indeed works as a cloaking device. The arguments above have been formulated such that they apply not only to the two-dimensional structure shown in Fig. 2, but also its three-dimensional generalization.

6. RAY-TRACING SIMULATIONS

To test and demonstrate our findings, we have programmed the cloak outlined above into our custom ray-tracer Dr TIM [43,44]. The ability to simulate light-ray transmission through glenses, and the ability to map between positive and negative space, is already part of Dr TIM [31]. This enabled us to visualize the view through the cloak.

Our simulations represent a number of physical effects incorrectly. First of all, the calculation of shadows is greatly simplified: surfaces are either shadow-throwing or not, and if there is a shadow-throwing surface in the straight line between a point on another surface and one of the point light sources, then that shadow-throwing surface casts a shadow on that point on the other surface. This simple treatment does not correctly represent the effect of surfaces that change the direction of transmitted light rays. Transmission through the glenses neglects absorption [34] and diffraction effects associated with the realization in the form of a Gabor superlens.

The cloak was programmed by defining the (physical-space) positions of the vertices of all surfaces that form the cloak, and also their EM-space counterparts. We then derived imaging requirements from the vertex positions in the two spaces; for example, glens G_{01} must image vertex position V'_{145} in negative space to position V_{145} in positive space [see Fig. 3(a)]. Using the procedure described in Appendix A, Dr TIM then determines the glens parameters from these imaging requirements.

Figure 5 shows that, within the limitations of our simulation, the cloak design works: the inner cube, and the sphere placed inside it, appear at reduced size, while any object behind the cloak is seen in the same direction as it would be without the cloak (but slightly dimmer, as all glens surfaces were made to be slightly absorbing in order to become visible in the simulations). Figure 6 shows the cloak working from a different virtual camera position, consistent with the cloak's omnidirectionality. Figure 6(a) differs from Fig. 5(b) only in the camera direction; in Fig. 6(b) the camera direction is the same as in Fig. 6(a), but the cloak is different in that the inner cube is smaller in EM space, so the inner cube and the sphere inside it appear reduced to a different apparent size, demonstrating that the reduction factor can, in principle, be chosen arbitrarily.

7. DISCUSSION AND CONCLUSIONS

Glenses are defined as idealized interfaces that change light-ray direction precisely as required, without offsetting light rays or introducing loss. This paper is about an omnidirectional cloak made from glenses (of which a few are lenses); if the glenses work as defined, then the cloak is perfect, as demonstrated by the simulations in the previous section.

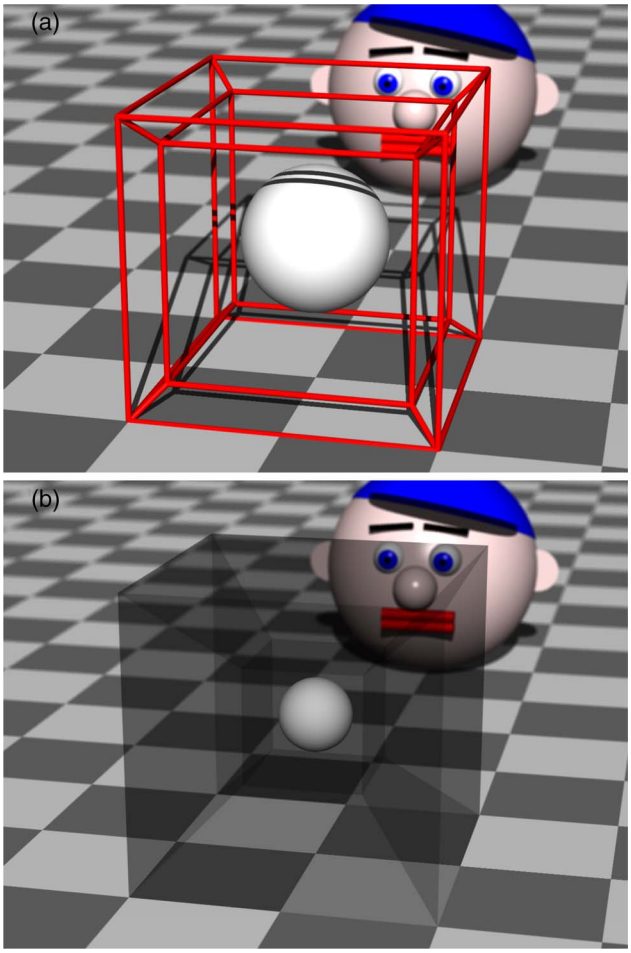

Fig. 5. Simulation of the cubic glens cloak. (a) A cylinder frame indicates the structure of the cloak. Wherever two or more glenses meet, a red cylinder is placed. The effect of the glenses is not simulated, which is why the sphere placed inside the central cube can be seen at its actual size. (b) When the effect of the glenses is simulated (and the cylinder frame removed), the effect of the cloak can be seen. The sphere inside the cloak is seen at a fraction of its actual size. The head behind the cloak is partially seen through the cloak, but appears in its actual position and at its actual size. The glenses have been made slightly absorbing so that the cloak can just be seen. The figure was calculated for $L = 2$ (in units of the floor-tile side length), $a = 0.8$, and $a' = 0.4$, which means the central cube appears to be half (a'/a) of its actual size. The simulation was performed with an extended version of Dr TIM [43,44].

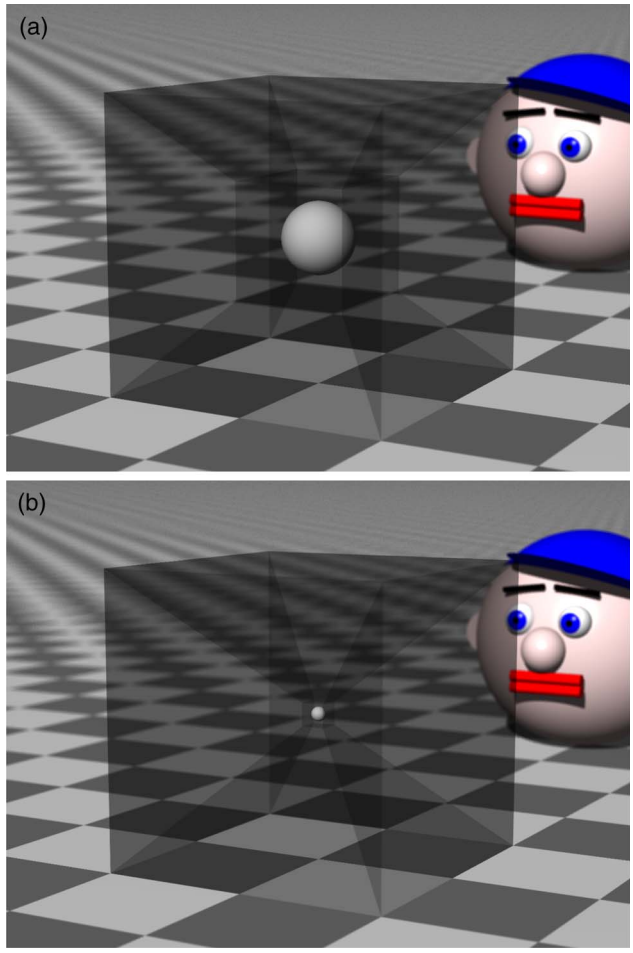

Fig. 6. Cubic glens cloak. (a) The same as the cloak shown in Fig. 5(a), but seen from a different direction. (b) Like (a), but with the parameters chosen such that the EM-space size of the inner cube is one-tenth of its physical-space size, so it appears to be a tenth of its actual size ($a' = 0.08$; like before, $a = 0.8$). The simulation was performed with an extended version of Dr TIM [43,44].

However, Gabor superlenses—the only experimental realization of pixelated glenses to date—suffer from imperfections, which would affect the functioning of any cloak built from them. One imperfection is the Gabor superlenses' limited field of view, which translates into a limited field of view of the cloak, which is therefore not omnidirectional. Another imperfection is that not all transmitted light changes direction as required. Such light either leads to additional images (if it is allowed to pass through the cloak) or a reduced transmission coefficient (if it is absorbed). Note that the fraction of light that passes through such a cloak as desired gets smaller as the factor by which the central square (cube) appears shrunk increases, just like in the cloak made from homogeneous glenses [38]. A third imperfection is the limited quality of the image formed by Gabor superlenses, which is due to a combination of fundamental effects (diffraction, pixel visibility) and practical effects (aberrations of the simple lens design, dispersion, etc.). This optical quality of the image formed by individual Gabor superlenses will need to improve significantly before imaging through combinations of such devices becomes visually palatable. Our current optical engineering efforts are aimed at making those and other improvements, and ultimately at building pixelated TO devices as a direct test of practical realizability.

In Section 2 it was pointed out that glenses perform light-ray-direction changes that, unless accompanied by an offset, can result in wave-optically forbidden light-ray fields, which is why practical realizations of glenses need to offset the rays. This can be seen as a violation of Liouville's theorem: any bundle of parallel rays incident on the cloak's inner cube in EM space will be altered by the cloak such that, inside the inner cube (in physical space), the rays have the same direction

but their distance has been stretched. In direction space, each ray is unchanged, but in position space the volume of the beam has been magnified, resulting in a change in phase-space volume. Upon transmission through the remainder of the cloak, the phase-space volume gets restored to its original size. Such a light beam would, in the simplest case, enter the inner cube by passing first through the glens at a face of the outer cube and then the glens at the corresponding face of the inner cube, but the combination of these two glenses, which share a nodal point, is precisely the glens telescope discussed in Ref. [31], where it is pointed out that such a device violates Liouville's theorem.

One of the macroscopic cloaks listed in Section 1 [12] comprises a simple series of lenses. These lenses image any object seen through all four lenses back to its original position, so such an object is seen undistorted. The cloak has been labeled "paraxial" as it only works for rays that travel close to the optical axis of the lenses. An interesting exercise would be to add glenses around these lenses such that the cloak becomes omnidirectional. It is not clear whether or not this is possible.

More desirable still would be to design TO devices made purely from lenses. Such a device would avoid the difficulties in manufacturing glenses, or even metamaterials; it would also avoid the limitations of glenses (such as diffraction and loss) and metamaterials (limited wavelength range, loss, etc.). It would also be intellectually satisfying by realizing the exotic concept of TO—developed in the context of metamaterials—with components as familiar as lenses. Our result constitutes a step in this direction.

APPENDIX A: CALCULATING GLENS PARAMETERS FROM TWO PAIRS OF CONJUGATE POINTS

We used our custom ray-tracer Dr TIM [44] to simulate the view through the cloak described in this paper. The parameters of the glenses that form the cloak have not been programmed into Dr TIM, but instead a procedure by which these parameters are being calculated from the cloak's imaging properties. This requires finding the parameters of a glens, given the glens plane and two conjugate pairs of points, Q^- and Q^+, and R^- and R^+ (see Fig. 7). The glens plane is given in terms of a position in the glens plane, and the normalized normal to the plane, $\hat{\mathbf{a}}$, which is also the direction of the optical axis. We use the geometry functionality already built into Dr TIM, which includes the capability to calculate the positions where straight lines intersect and the orthographic projection of positions into planes, to achieve this, as follows.

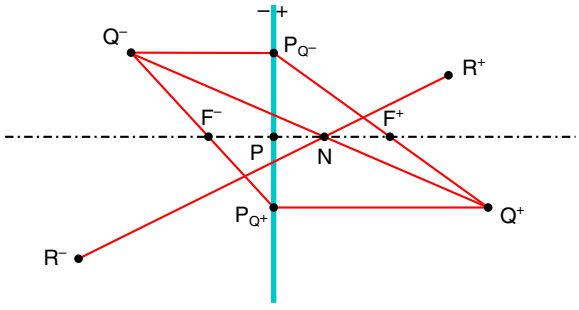

Fig. 7. Construction of the cardinal points of a glens in a given plane from two pairs of conjugate points. The glens images Q^- and Q^+ into each other, and R^- and R^+. P_{Q^-} and P_{Q^+} are the orthographic projections of positions Q^- and Q^+ into the glens plane.

We first calculate the position of the nodal point, N, which is the position where the straight lines through Q^- and Q^+ and through R^- and R^+ intersect. If these lines do not intersect, then the required glens does not exist. In Dr TIM's implementation, a Java exception is thrown in this case.

Once the nodal point has been found, the principal point P can be calculated: it is simply the orthographic projection of N into the glens plane.

Next, we can calculate the positive focal length, f^+, which is the a coordinate of the positive focal point, F^+. F^+ can be constructed as the point where the optical axis intersects the straight line between Q^+ and P_{Q^-}, the orthographic projection into the glens plane of Q^-. As before, if no such intersection exists, a Java exception is thrown. The corresponding focal length is then

$$f^+ = (\mathbf{F}^+ - \mathbf{P}) \cdot \hat{\mathbf{a}}, \tag{A1}$$

where $\mathbf{F}^+$ and $\mathbf{P}$ are the position vectors that correspond to F^+ and P. The negative focal length, f^-, can be calculated similarly by calculating F^- as the intersection of the straight line through P_{Q^+} and Q^- with the optical axis, and then calculating the a coordinate of F^-.

Finally, Dr TIM checks that the glens with the calculated parameters indeed images both object–image pairs as required.

This procedure is implemented in the `setParametersUsingTwoConjugatePairs` method of the GlensHologram class in the `optics.raytrace.surfaces` package. The complete source code of Dr TIM is available online [45].

Funding. Engineering and Physical Sciences Research Council (EPSRC) (EP/K503058/1, EP/M010724/1); Grantová Agentura České Republiky (GACR) (P201/12/G028).

REFERENCES AND NOTES

1. U. Leonhardt, "Optical conformal mapping," Science **312**, 1777–1780 (2006).
2. J. B. Pendry, D. Schurig, and D. R. Smith, "Controlling electromagnetic fields," Science **312**, 1780–1782 (2006).
3. D. Schurig, J. J. Mock, B. J. Justice, S. A. Cummer, J. B. Pendry, A. F. Starr, and D. R. Smith, "Metamaterial electromagnetic cloak at microwave frequencies," Science **314**, 977–980 (2006).
4. R. Liu, C. Ji, J. J. Mock, J. Y. Chin, T. J. Cui, and D. R. Smith, "Broadband ground-plane cloak," Science **323**, 366–369 (2009).
5. J. Valentine, J. Li, T. Zentgraf, G. Bartal, and X. Zhang, "An optical cloak made of dielectrics," Nat. Mater. **8**, 568–571 (2009).
6. T. Ergin, N. Stenger, P. Brenner, J. B. Pendry, and M. Wegener, "Three-dimensional invisibility cloak at optical wavelengths," Science **328**, 337–339 (2010).
7. N. Landy and D. R. Smith, "A full-parameter unidirectional metamaterial cloak for microwaves," Nat. Mater. **12**, 25–28 (2013).
8. X. Chen, Y. Luo, J. Zhang, K. Jiang, J. B. Pendry, and S. Zhang, "Macroscopic invisibility cloaking of visible light," Nat. Commun. **2**, 176 (2011).
9. B. Zhang, Y. Luo, X. Liu, and G. Barbastathis, "Macroscopic invisibility cloak for visible light," Phys. Rev. Lett. **106**, 033901 (2011).

10. H. Chen, B. Zheng, L. Shen, H. Wang, X. Zhang, N. Zheludev, and B. Zhang, "Ray-optics cloaking devices for large objects in incoherent natural light," Nat. Commun. **4**, 2652 (2013).
11. J. C. Howell, J. B. Howell, and J. S. Choi, "Amplitude-only, passive, broadband, optical spatial cloaking of very large objects," Appl. Opt. **53**, 1958–1963 (2014).
12. J. S. Choi and J. C. Howell, "Paraxial ray optics cloaking," Opt. Express **22**, 29465–29478 (2014).
13. R. Schittny, M. Kadic, S. Guenneau, and M. Wegener, "Experiments on transformation thermodynamics: molding the flow of heat," Phys. Rev. Lett. **110**, 195901 (2013).
14. R. Hu, X. Wei, J. Hu, and X. Luo, "Local heating realization by reverse thermal cloak," Sci. Rep. **4**, 3600 (2014).
15. B.-I. Popa, L. Zigoneanu, and S. A. Cummer, "Experimental acoustic ground cloak in air," Phys. Rev. Lett. **106**, 253901 (2011).
16. N. Stenger, M. Wilhelm, and M. Wegener, "Experiments on elastic cloaking in thin plates," Phys. Rev. Lett. **108**, 014301 (2012).
17. S. Brûlé, E. H. Javelaud, S. Enoch, and S. Guenneau, "Experiments on seismic metamaterials: molding surface waves," Phys. Rev. Lett. **112**, 133901 (2014).
18. H. Hashemi, B. Zhang, J. D. Joannopoulos, and S. G. Johnson, "Delay-bandwidth and delay-loss limitations for cloaking of large objects," Phys. Rev. Lett. **104**, 253903 (2010).
19. H. Hashemi, A. Oskooi, J. D. Joannopoulos, and S. G. Johnson, "General scaling limitations of ground-plane and isolated-object cloaks," Phys. Rev. A **84**, 023815 (2011).
20. H. Hashemi, C.-W. Qiu, A. P. McCauley, J. D. Joannopoulos, and S. G. Johnson, "Diameter-bandwidth product limitation of isolated-object cloaking," Phys. Rev. A **86**, 013804 (2012).
21. J. C. Halimeh, T. Ergin, J. Mueller, N. Stenger, and M. Wegener, "Photorealistic images of carpet cloaks," Opt. Express **17**, 19328–19336 (2009).
22. B. Zhang, T. Chan, and B.-I. Wu, "Lateral shift makes a ground-plane cloak detectable," Phys. Rev. Lett. **104**, 233903 (2010).
23. J. C. Halimeh, R. Schmied, and M. Wegener, "Newtonian photorealistic ray tracing of grating cloaks and collation-function-based cloaking-quality assessment," Opt. Express **19**, 6078–6092 (2011).
24. J. C. Halimeh and M. Wegener, "Photorealistic ray tracing of free-space invisibility cloaks made of uniaxial dielectrics," Opt. Express **20**, 28330–28340 (2012).
25. A. J. Danner, "Visualizing invisibility: metamaterials-based optical devices in natural environments," Opt. Express **18**, 3332–3337 (2010).
26. C.-W. Qiu, A. Akbarzadeh, T. Han, and A. J. Danner, "Photorealistic rendering of a graded negative-index metamaterial magnifier," New J. Phys. **14**, 033024 (2012).
27. A. C. Hamilton and J. Courtial, "Metamaterials for light rays: ray optics without wave-optical analog in the ray-optics limit," New J. Phys. **11**, 013042 (2009).
28. J. Courtial, "Ray-optical refraction with confocal lenslet arrays," New J. Phys. **10**, 083033 (2008).
29. A. C. Hamilton and J. Courtial, "Generalized refraction using lenslet arrays," J. Opt. A **11**, 065502 (2009).
30. J. Courtial and T. Tyc, "Generalised laws of refraction that can lead to wave-optically forbidden light-ray fields," J. Opt. Soc. Am. A **29**, 1407–1411 (2012).
31. G. J. Chaplain, G. Macauley, J. Bělín, T. Tyc, E. N. Cowie, and J. Courtial, "Ray optics of generalized lenses," J. Opt. Soc. Am. A **33**, 962–969 (2016).
32. R. F. Stevens and T. G. Harvey, "Lens arrays for a three-dimensional imaging system," J. Opt. A **4**, S17–S21 (2002).
33. J. Courtial, "Standard and non-standard metarefraction with confocal lenslet arrays," Opt. Commun. **282**, 2634–2641 (2009).
34. T. Maceina, G. Juzeliūnas, and J. Courtial, "Quantifying metarefraction with confocal lenslet arrays," Opt. Commun. **284**, 5008–5019 (2011).
35. Rowlux Illusion Film, which has a structure that is closely related to that of telescope windows, is inexpensive and available on meter scales from Rowland Technologies Inc.; see "Rowlux illusion film (data sheet)," http://www.rowtec.com/literaturedownloads.html.
36. S. Oxburgh and J. Courtial, "Perfect imaging with planar interfaces," J. Opt. Soc. Am. A **30**, 2334–2338 (2013).
37. S. Oxburgh, C. D. White, G. Antoniou, E. Orife, and J. Courtial, "Transformation optics with windows," Proc. SPIE **9193**, 91931E (2014).
38. S. Oxburgh, C. D. White, G. Antoniou, E. Orife, T. Sharpe, and J. Courtial, "Large-scale, white-light, transformation optics using integral imaging," J. Opt. **18**, 044009 (2016).
39. J. Courtial, "Geometric limits to geometric optical imaging with infinite, planar, non-absorbing sheets," Opt. Commun. **282**, 2480–2483 (2009).
40. J. Courtial, S. Oxburgh, and T. Tyc, "Direct, stigmatic, imaging with curved surfaces," J. Opt. Soc. Am. A **32**, 478–481 (2015).
41. C. Hembd-Sölner, R. F. Stevens, and M. C. Hutley, "Imaging properties of the Gabor superlens," J. Opt. A **1**, 94–102 (1999).
42. D. Gabor, "Improvements in or relating to optical systems composed of lenticules," UK patent 541,753 (December 10, 1941).
43. D. Lambert, A. C. Hamilton, G. Constable, H. Snehanshu, S. Talati, and J. Courtial, "TIM, a ray-tracing program for METATOY research and its dissemination," Comput. Phys. Commun. **183**, 711–732 (2012).
44. S. Oxburgh, T. Tyc, and J. Courtial, "Dr TIM: ray-tracer TIM, with additional specialist capabilities," Comput. Phys. Commun. **185**, 1027–1037 (2014).
45. "TIM: a raytracer for forbidden optics," http://sourceforge.net/projects/timray/.